THE JOURNAL OF BIOLOGICAL CHEMISTRY VOL. 289, NO. 49, pp. 34175–34188, December 5, 2014

A Type IV Translocated *Legionella* Cysteine Phytase Counteracts Intracellular Growth Restriction by Phytate[S]

Received for publication, July 2, 2014, and in revised form, August 26, 2014 Published, JBC Papers in Press, October 22, 2014, DOI 10.1074/jbc.M114.592568

Stephen Weber[‡], Christian U. Stirnimann[§1,2], Mara Wieser[§1], Daniel Frey[§1], Roger Meier[¶], Sabrina Engelhardt[‖], Xiaodan Li[§1], Guido Capitani[§1], Richard A. Kammerer[§1], and Hubert Hilbi[‡3]**

*From the [‡]Max von Pettenkofer Institute, Department of Medicine, Ludwig-Maximilians University Munich, 80336 Munich, Germany, the [§]Laboratory of Biomolecular Research, Department of Biology and Chemistry, Paul Scherrer Institute, 5232 Villigen, Switzerland, the [¶]Scientific Center for Optical and Electron Microscopy, ETH Zurich, 8093 Zurich, Switzerland, the [‖]Institute of Veterinary Physiology and Zurich Center for Integrative Human Physiology (ZIHP), Vetsuisse Faculty, University of Zurich, 8057 Zurich, Switzerland, and the **Institute of Medical Microbiology, Department of Medicine, University of Zurich, 8006 Zurich, Switzerland*

Background: *Legionella* governs pathogen-host interactions by translocating ~300 "effector" proteins through a type IV secretion system.
Results: The hitherto unrecognized effector LppA is a phytase that counteracts intracellular bacterial growth restriction by phytate.
Conclusion: The chelator phytate is a bacteriostatic component of cell-autonomous immunity, which is degraded by a bacterial effector.
Significance: *Legionella* LppA represents the first translocated phytase and a potential therapeutic target.

The causative agent of Legionnaires' pneumonia, *Legionella pneumophila*, colonizes diverse environmental niches, including biofilms, plant material, and protozoa. In these habitats, *myo*-inositol hexakisphosphate (phytate) is prevalent and used as a phosphate storage compound or as a siderophore. *L. pneumophila* replicates in protozoa and mammalian phagocytes within a unique "*Legionella*-containing vacuole." The bacteria govern host cell interactions through the Icm/Dot type IV secretion system (T4SS) and ~300 different "effector" proteins. Here we characterize a hitherto unrecognized Icm/Dot substrate, LppA, as a phytate phosphatase (phytase). Phytase activity of recombinant LppA required catalytically essential cysteine (Cys^{231}) and arginine (Arg^{237}) residues. The structure of LppA at 1.4 Å resolution revealed a mainly α-helical globular protein stabilized by four antiparallel β-sheets that binds two phosphate moieties. The phosphates localize to a P-loop active site characteristic of dual specificity phosphatases or to a non-catalytic site, respectively. Phytate reversibly abolished growth of *L. pneumophila* in broth, and growth inhibition was relieved by overproduction of LppA or by metal ion titration. *L. pneumophila* lacking *lppA* replicated less efficiently in phytate-loaded *Acanthamoeba castellanii* or *Dictyostelium discoideum*, and the intracellular growth defect was complemented by the phytase gene. These findings identify the chelator phytate as an intracellular bacteriostatic component of cell-autonomous host immunity and reveal a T4SS-translocated *L. pneumophila* phytase that counteracts intracellular bacterial growth restriction by phytate. Thus, bacterial phytases might represent therapeutic targets to combat intracellular pathogens.

Legionella spp. are ubiquitous water-borne bacteria that colonize diverse environmental niches, including biofilms, plant material, and protozoa (1–4). In free living amoebae and mammalian phagocytes, *Legionella pneumophila* replicates within a "*Legionella*-containing vacuole" (LCV),[4] employing the Icm/Dot type IV secretion system (T4SS) and ~300 different "effector" proteins (5–7). Some *L. pneumophila* Icm/Dot substrates target and subvert pivotal regulators of eukaryotic signal transduction and vesicle trafficking, such as small GTPases (8–13) or phosphoinositide (PI) lipids (14–16). Several *Legionella* effectors anchor to the LCV membrane by specifically binding to the phosphorylated phosphatidylinositol (PtdIns) headgroup of PI lipids, namely PtdIns(4)P (17–22) and PtdIns(3)P (23–25), which are implicated in secretory and endosomal vesicle trafficking, respectively. Moreover, *L. pneumophila* produces two non-homologous Icm/Dot-translocated PI 3-phosphatases, SidF and SidP, which might modulate the LCV PI pattern (26, 27). SidF localizes to the LCV membrane and hydrolyzes *in vitro* the phagosomal/endosomal PIs PtdIns(3,4)P_2 and PtdIns(3,4,5)P_3, possibly yielding PtdIns(4)P on LCVs directly or through the activity of the host PI 5-phosphatase OCRL1

[S] This article contains supplemental Movies S1–S4.

[1] Supported by the Paul Scherrer Institute and grants from the Swiss National Science Foundation (SNF).

[2] Present address: NEXUS Personalized Health Technologies, Theragnostics Discovery Unit, Otto-Stern-Weg 7, ETH Zurich, 8093 Zurich, Switzerland.

[3] Work in this author's group was supported by the Max von Pettenkofer Institute, Ludwig-Maximilians University Munich, the German Research Foundation (Deutsche Forschungsgemeinschaft Grants HI 1511/1-1, SPP 1316, and SPP 1580), and the German Ministry of Education and Research (BMBF) in the context of the Infect-ERA initiative (project EUGENPATH). To whom correspondence should be addressed: Institute of Medical Microbiology, Dept. of Medicine, University of Zurich, 8006 Zurich, Switzerland. Tel.: 41-44-634-2650; Fax: 41-44-634-4906; E-mail: hilbi@imm.uzh.ch.

[4] The abbreviations used are: LCV, *Legionella*-containing vacuole; AYE, ACES yeast extract; T4SS, type IV secretion system; PI, phosphoinositide; PtdIns, phosphatidyl-inositol; PTEN, phosphatase and tensin homologue deleted on chromosome 10; PTP, protein-tyrosine phosphatase; Kan, kanamycin; β-ME, β-mercapthoethanol; MOI, multiplicity of infection.

TABLE 1
Strains and plasmids

Strain/plasmid	Relevant properties[a]	Source/Reference
E. coli		
TOP10		Invitrogen
BL21		Novagen
L. pneumophila		
GS3011	*L. pneumophila* JR32 *icmT3011*::Kan^R (Δ*icmT*)	Ref. 58
JR32	Virulent *L. pneumophila* serogroup 1 strain Philadelphia-1	Ref. 59
RM01	*L. pneumophila* JR32 *lpg2819*::Kan^R (Δ*lppA*)	This work
Plasmids		
pAK7	Expression of N-terminal His tag fusions, pET-28a(+)-based	This work
pCR33	*Legionella* expression vector, Δ*mobA*, RBS, M45-(Gly)$_5$, Cam^R (=pMMB207-C-RBS-M45)	Ref. 17
pCR76	pMMB207-C-P$_{tac}$-RBS-*gfp*-RBS-MCS	Ref. 25
pET-28a(+)	Expression of N-terminal His tag fusions; P$_{T7}$; Kan^R	Novagen
pGEX-6P-1	GST expression vector	GE Healthcare
pGEX-4T-1	GST expression vector	GE Healthcare
pGEM-T-easy	Cloning vector	Promega
pLAW344	*L. pneumophila* suicide vector	Ref. 60
pMMB207-C	*Legionella* expression vector, Δ*mobA*, w/o RBS, Cam^R	Ref. 46
pNT28	pMMB207-C-RBS-*gfp* (constitutive *gfp*)	Ref. 44
pPhyA	Synthetic construct of *S. ruminantium phyA* gene	This work
pRM1	pMMB207-C-RBS-M45-*lppA*	This work
pRM2	pGEM-T-easy-*lppA*$_{down}$_Kan^R_*lppA*$_{up}$	This work
pRM3	pLAW344-*lppA*$_{down}$_Kan^R_*lppA*$_{up}$	This work
pRM4	pGEX-4T-1-*lppA*	This work
pRM9	pGEX-6P-1-*lppA*$_{Δ1–16}$	This work
pSE7	pGEX-6P-1-*lppA*$_{Δ1–16,}$ C231A	This work
pSE8	pGEX-6P-1-*lppA*$_{Δ1–16,}$ K235A	This work
pSE9	pGEX-6P-1-*lppA*$_{Δ1–16,}$ R237A	This work
pSE10	pGEX-6P-1-*lppA*$_{Δ1–16,}$ G236D	This work
pSH97	pMMB207-C-RBS-*cyaA* (including polylinker)	Ref. 25
pSH100	pMMB207-C-*cyaA-ralF*	Ref. 25
pSH108	pMMB207-C-*cyaA-lppA*	This work
pSU4	GFP-SidC$_{p4C}$ in pDXA, G418^R	Ref. 18
pSW001	pMMB207-C-P$_{tac}$-*dsred* Δ*lacI*^{q} (constitutive *dsred*)	Ref. 61
pSW013	pGEX-4T-1-*lpnE*	Ref. 23
pWS11	pET-28a(+)-*lppA*$_{21–314}$	This work
pWS25	pGEX-6P-1-*phyA*$_{Δ1–16}$	This work
pWS31	pMMB207-C-RBS-*gfp*-RBS-*lppA*	This work

[a] Cam, chloramphenicol; G418, Geneticin.

(23). SidP hydrolyzes *in vitro* the endosomal PI lipids PtdIns(3)P and PtdIns(3,5)P_2, thereby possibly contributing to the evasion of the endocytic pathway by the LCV. By virtue of their phosphorylated inositol headgroups, PIs bear high resemblance to phytate (*myo*-inositol hexakisphosphate) and lower inositol phosphates.

Phytate is used as the major phosphorus storage compound by plants and is the most abundant organic phosphorus compound in the environment (28–30). Protozoa also synthesize phytate, and in particular, the social soil amoeba *Dictyostelium discoideum* produces the compound in millimolar quantities (31–33). Phytate is rather inert, yet phosphorus mineralization is catalyzed in a stepwise manner by specific phosphohydrolases (phytases), which are produced by a wide range of bacteria (29). The plant pathogen *Xanthomonas oryzae* uses a secreted phytase as a virulence factor for growth on phytate as the sole phosphate source (34). In addition to serving as a source of phosphorus, carbon, and energy, phytate may also play a role in bacterial iron acquisition by chelating metal ions. Accordingly, *Pseudomonas aeruginosa* employs phytate as an iron siderophore (35, 36). Phytate is also a prominent anti-nutrient able to complex several metal ion micronutrients, thus restricting their bioavailability (37).

Based on their sequence similarities, phytases are classified as four different groups comprising histidine acid phosphatases, purple acid phosphatases, β-propeller phosphatases, and cysteine phytases (29, 38, 39). The conserved amino acid motif CX_5R is a hallmark of the "P-loop" (phosphate-binding) catalytic site of the prototypic cysteine phytase PhyA in *Selenomonas ruminantium* (39) as well as of eukaryotic and prokaryotic PI phosphatases, such as PTEN (phosphatase and tensin homologue deleted on chromosome 10), *L. pneumophila* SidF and SidP (26, 27, 40), dual specificity Ser/Thr and Tyr protein phosphatases (DSP) (41), and the triple specificity DSP/PI phosphatase MptpB from *Mycobacterium tuberculosis* (42, 43).

By using the phosphatase consensus sequence HC*XX*G*XX*RT as a search motif, we identified an *L. pneumophila* cysteine phytase. The phytase, termed LppA, hydrolyzes phytate and PIs *in vitro* and is translocated by the Icm/Dot T4SS into host cells, where it counteracts intracellular bacterial growth restriction by the chelator phytate.

EXPERIMENTAL PROCEDURES

Bacteria, Cells, and Growth Conditions—L. pneumophila strains (Table 1) were grown for 3 days on charcoal yeast extract agar plates buffered with *N*-(2-acetamido)-2-aminoethane-sulfonic acid. Liquid cultures were inoculated in AYE medium at an A_{600} of 0.1 and grown at 37 °C to an A_{600} of 3.0–3.4 (~21–22 h) (17). Chloramphenicol was added at 5 μg/ml to select for pMMB207-C-derived plasmids. Murine RAW 264.7 macrophages were cultivated in RPMI 1640 medium supplemented with 10% FCS and 2 mM L-glutamine. *Acanthamoeba castellanii* (ATCC 30234) and *D. discoideum* amoebae were propagated as described (44).

TABLE 2
Oligonucleotides used in this study
Restriction sites are underlined.

Oligonucleotide	Sequence (5′–3′)	Comments
oCR149	GCTGTTGACAATTAATCATCGG	pMMB207 fo (sequencing)
oCR150	CGTTCTGATTTAATCTGTATCAGGC	pMMB207 re (sequencing)
oCR161	AAAAACGCGGATCCATGAGCTTTAAAGGATTTAAAGTG	5′ of *lppA*, BamHI
oCR162	AAAAACGCTCTAGACTATTACTAGATATTGAGCTTTTTCCATTC	3′ of *lppA*, XbaI
oAK7fo	GGACGCTCATGAAAAAAAATCACCACCATCATCACCACCTAGTTCCGCGTGGATCCGAATGG	BspHI/BamHI
oAK7re	CCATTCGGATCCACGCGGAACTAGGTGGTGATGATGGTGGTGATTTTTTTTCATGAGCGTCC	BamHI/BspHI
oKan3′	TCACTTTCTGGCTGGATGATGG	5′ out of Kan^R (deletion)
oKan5′	GAATATGGCTCATAACACCCC	3′ out of Kan^R (deletion)
oRM1	AAAAACGCGGATCCCATCTAGTGCCATTTGCAAG	5′ of *lppA* downstream region (deletion), BamHI
oRM2	TTAGCGATACCTGGAAATAAG	3′ of *lppA* downstream region (deletion)
oRM3	GGTCATAACGATGCAAATAGTAG	5′ of *lppA* upstream region (deletion)
oRM4	AAAAACGCGGATCCAATAAATCCTTTTTAAATCCCTAAAGATG	3′ of *lppA* upstream region (deletion), BamHI
oRM5	AAAAACGCGGATCCATGAGCTTTAAAGGATTTAAAG	5′ of *lppA*, BamHI
oRM6	AAAAACGCGTCGACCTAGATATTGAGCTTTTTCCATTC	3′ of *lppA*, SalI
oRM7	GGCTGTCTGATTTTCCTCAAG	3′ of *lppA* downstream region
oRM8	CTGCCCGAATGGTATCAG	5′ of *lppA* upstream region
oRM13	AAAAACGCGGATCCCAAAGTTATGCCTCTAAATTG	5′ of $lppA_{\Delta 1-16}$, BamHI
oSE7	GGTATCATGTCCACGCCCGTGGCGGGAAAGGC	5′ of *lppA* C231A
oSE8	GCCTTTCCCGCCACGGGCGTGGACATGATACC	3′ of *lppA* C231A
oSE9	GCCGTGGCGGGGCAGGCCGTACGACG	5′ of *lppA* K235A
oSE10	CGTCGTACGGCCTGCCCCGCCACGGC	3′ of *lppA* K235A
oSE11	CGTGGCGGGAAAGGCGCTACGACGACTGTTTTTGC	5′ of *lppA* R237A
oSE12	GCAAAAACAGTCGTCGTAGCGCCTTTCCCGCCACG	3′ of *lppA* R237A
oSE13	CCGTGGCGGGAAAGACCGTACGACGACTG	5′ of *lppA* G236D
oSE14	CAGTCGTCGTACGGTCTTTCCCGCCACGG	3′ of *lppA* G236D
oWS25	AGTTATGGATCCAAATTGGCATCCTCC	5′ of $lppA_{21-314}$, BamHI (crystallization)
oWS26	CTAGATGTCGACTTATTACCATTCTGACCA	3′ of $lppA_{21-314}$, SalI (crystallization)
oWS73	AAAAAAGGATCCGCCAAGGCGCCGGAGCAGACGGTGACGG	5′ of *phyA*, BamHI
oWS91	AAAAAAGTCGACCTACTTCGCCGGATGGCTCTTGAGCCAG	3′ of *phyA*, SalI

Chromosomal Deletion of lppA, Plasmid Construction, and Site-directed Mutagenesis—All plasmids used are listed in Table 1. DNA manipulations were performed according to standard protocols, and plasmids were isolated using kits from Qiagen or Macherey-Nagel. All PCR fragments were sequenced.

The chromosomal deletion of *lppA* was performed by double homologous recombination as described (44); 500 bp downstream and upstream fragments were amplified by PCR using the primer pairs oRM1/oRM2 and oRM3/oRM4, respectively (Table 2). Both fragments were inserted by a four-way ligation into a pGEM-T-easy vector with a kanamycin resistance (Kan^R) cassette in between using BamHI sites and adenosine overhangs, yielding plasmid pRM2. Clones were analyzed by restriction digestion and sequencing. The Kan^R cassette flanked by upstream and downstream fragments was transferred into the pLAW344 suicide plasmid using NotI, yielding plasmid pRM3. *L. pneumophila* JR32 was transformed by electroporation with pRM3 and selected for Kan^R and Suc^S colonies. Positive clones were tested by PCR using the primer pairs oRM7/oKan3′ and oRM8/oKan3′.

Translational CyaA and M45 fusion proteins of *lppA* were constructed by PCR amplification of the corresponding DNA. The fragments were cut with appropriate restriction enzymes and inserted into pSH97, pMMB207-C-RBS-M45, or pMMB207-C-RBS-*gfp*-RBS, using the oligonucleotides oCR161/oCR162 or oRM5/oRM6, yielding plasmids pSH108, pRM1, and pWS31, respectively. Translational GST fusion proteins of *lppA* were constructed as above with the exception that the first 16 amino acids of the LppA protein were deleted by PCR amplification of the *lppA* template. The *lppA* fragment was cloned into pGEX-6P-1 using the oligonucleotides oRM13 and oRM6, yielding plasmid pRM9.

The *S. ruminantium* phytase gene *phyA* (39) was synthesized by GenScript USA Inc. and delivered in commercial vector pUC57-Kan with flanking BamHI and SalI restriction sites. In the design, the intrinsic SalI site of the gene was removed by a silent single base substitution, maintaining the original amino acid sequence. The *phyA* gene was cloned with BamHI and SalI into pGEX-6P-1, yielding pWS25.

Site-directed mutagenesis of the P-loop residue C231A, K235A, G236D, or R237A of $lppA_{\Delta 1-16}$ was performed with the QuikChange Lightning multisite-directed mutagenesis kit (Agilent Technologies) according to the manufacturer's instructions. PCR amplification was carried out using primers carrying the corresponding point mutations to yield the plasmids pSE7 to pSE10. The methylated template pRM9 was digested with DpnI.

Vector pAK7 was constructed by PCR amplification of the complementary primers pAK7fo/pAK7re, followed by restriction digestion with BamHI/BspHI, and insertion into pET-28a(+) cut with BamHI/NcoI (compatible with BspHI). The plasmid pWS11 was cloned by BamHI/SalI insertion of the PCR product of oWS25 and oWS26 into pAK7.

Phosphate Release and Protein-Lipid Overlay Assay—GST fusion proteins were purified as described previously (25). Phytate (phytic acid sodium salt hydrate) was obtained from Sigma-Aldrich, and synthetic dioctyl PI and inositol phosphates were purchased from Echelon Biosciences Inc. (Salt Lake City, UT). Phosphate release from phytate or PI substrates was assayed by a malachite green assay (protein-tyrosine phosphatase (PTP) assay kit, Sigma-Aldrich) in a total volume of 50 μl/well in a 384-well plate (Greiner) at 25 °C. Substrates were prepared in 25 μl of assay buffer (100 mM Tris-HCl, 120 mM NaCl, pH 7.4). To initiate the reaction, 25 μl of enzyme solution in assay buffer (0.05–5 μg of protein) was added and mixed three times rapidly without blowing out. 25 μl of the malachite green acidic dye and vanadate ion complex (mixed 100:1 at least 30 min before use) were added to terminate reactions. The

color was developed for 20 min, and absorbance was measured at 620 nm with a FLUOstar plate reader (BMG Labtech). All values for a series were standardized against the zero reading (enzyme solution and malachite green mixed, followed by the addition of substrate solution), and 2–4 samples were used for each time point. A standard reference curve for phosphate release was generated using the 1 mM phosphate standard supplied with the kit.

The products of LppA from various PI lipids were assessed with PIP-strips (Echelon Biosciences Inc.) treated with 0.5 μg/ml LppA for 10 min. Membranes were washed three times for 10 min with PBS. Subsequent binding of GST-$SidC_{P4C}$ or GST-LpnE probes and anti-GST Western blots were carried out as described previously (17, 18). Peroxidase-labeled secondary antibodies were visualized by ECL (Amersham Biosciences).

Detection of LppA by Western Blot—30-ml AYE cultures of *L. pneumophila* wild type, Δ*lppA*, or wild type harboring vector pRM1 were grown overnight at 37 °C to early stationary phase. Cultures were standardized to an A_{600} of 3.0 with AYE and pelleted at 12,000 × *g* for 15 min. Supernatants were decanted to new tubes and centrifuged again; this was repeated once. 5 ml of cell-free supernatants of each strain were loaded with a dot blot apparatus onto a nitrocellulose membrane under vacuum suction. The bacterial pellets were suspended in 30 ml of Tris-buffered saline (TBS), and a 1.5-ml aliquot of each was boiled for 10 min at 95 °C. Cell debris was pelleted, and 500 μl of lysate for each strain was loaded onto a nitrocellulose membrane under vacuum suction. The membrane was blocked for 1 h in TBS containing 4% milk powder and stained for 1 h with an affinity-purified polyclonal anti-LppA antibody (1:500; GenScript), followed by an anti-rabbit HRP-tagged antibody (1:5,000) for 30 min.

Protein Purification and Crystallization—To produce $LppA_{21–314}$ for crystallization, plasmid pWS11 was transformed into chemically competent *E. coli* NiCo[DE3] (New England Biolabs) and plated on LB-Kan agar plates containing 50 μg/ml Kan. Several colonies were picked, transferred into 100 ml of LB medium containing 50 μg/ml Kan, and incubated overnight at 37 °C in an orbital shaker. 4 liters of ZYM5052-Kan autoinduction medium (for protein production by autoinduction in high density shaking cultures (45)) containing 50 μg/ml Kan were inoculated with 25 ml (1:40) of the overnight culture and grown at 37 °C for 7 h in a large orbital shaker. The temperature was subsequently lowered to 20 °C, and incubation was continued overnight. The cells were harvested by centrifugation at 5,000 rpm. Cell pellets were suspended in 100 ml of lysis buffer (50 mM Tris, pH 7.5, 500 mM NaCl, 10 mM imidazole, 10 mM β-mercapthoethanol (β-ME), 1 protease inhibitor mixture tablet (Complete EDTA-free, Roche Applied Science)) and lysed on ice using three 1-min 100% amplitude sonication pulses (Vibra-Cell sonication device (Sonics) equipped with a large preparative sonication tip). Soluble proteins were separated from cell debris by centrifugation (25,000 × *g*, 30 min), followed by filtration of the supernatant (0.45 μm).

Recombinant LppA was purified by immobilized metal affinity chromatography, followed by size exclusion chromatography, using an ÄKTA Xpress chromatography machine. The supernatant was loaded onto a 5-ml HisTrap crude FF column. The column was washed with 20 column volumes of wash buffer 1 (50 mM Tris, pH 7.5, 500 mM NaCl, 10 mM imidazole, 10 mM β-ME) and 20 column volumes of wash buffer 2 (50 mM Tris, pH 7.5, 500 mM NaCl, 60 mM imidazole, 10 mM β-ME). Recombinant LppA was eluted with 5 column volumes of elution buffer (50 mM Tris, pH 7.5, 500 mM NaCl, 500 mM imidazole, 10 mM β-ME). The eluted protein was injected to a 26/60 HiLoad Superdex200 size exclusion column (buffer: 50 mM Tris, pH 7.5, 500 mM NaCl, 10 mM β-ME). The total yield was 155 mg of pure LppA. The protein was concentrated to 5 mg/ml using a 10,000 molecular weight cut-off ultrafiltration concentrator (Millipore) and used for crystallization trials.

TABLE 3
Data collection and refinement statistics for LppA

Space group	P 1 2_1 1
Cell dimensions *a*, *b*, *c* (Å), β (degrees)	98.65 55.49 131.42 99.61
Resolution (Å)	50–1.4 (1.5–1.4)[a]
R_{meas} (%)	5.4 (82.8)
$I/\sigma I$	15.9 (2.3)
CC(1/2) (%)	99.9 (81.7)
Completeness (%)	96.0 (90.5)
Redundancy	4.5 (4.6)
Refinement	
Resolution (Å)	50.0–1.4
No. of reflections (test reflections)	264665 (1060)
R_{work}, R_{free} (%)	14.4, 16.9
No. of atoms	12052
Protein	10529
Ligand/ion	59
Water	1464
***B*-factors (Å^2)**	
Protein	23.8
Ligand/ion	19.5
Water	35.6
Root mean square deviations	
Bond lengths (Å)	0.007
Bond angles (degrees)	1.13
Ramachandran plot (Molprobity)	
Allowed (%)	1.9
Favored (%)	98.1

[a] Outermost resolution shell.

Crystallization experiments were carried out at the crystallization facility of the Swiss Light Source. Crystals were obtained with the sitting drop vapor diffusion method at 293 K, using a well solution containing 40 mM KH_2PO_4, pH 4.1, 16% PEG 8000, and 20% glycerol. Drops consisted of 1 μl of protein solution and 1 μl of well solution.

Data Collection and Structure Determination—Diffraction data from a single LppA crystal were collected at 100 K on a PILATUS 6M pixel detector at the Swiss Light Source beamline X10SA using an x-ray wavelength of 1.0000 Å. The data were processed using XDS (62) to a resolution of 1.4 Å. The structure was solved by molecular replacement and autorebuilt using PHENIX (63); four molecules per asymmetric unit were found using the monomeric structure of protein tyrosine phosphatase-like phytase from *Mitsuokella multacida* (Protein Data Bank code 3F41) as a search model. Refinement and manual model rebuilding were carried out with PHENIX and Coot (64), respectively. The model was validated using MolProbity (65); analysis with EPPIC (66) did not find any biologically relevant interfaces in the crystal lattice. Data collection and refinement statistics are shown in Table 3.

Translocation Assay—To determine translocation of LppA, adenylate cyclase fusion proteins were generated and used to

quantify the production of cAMP in the host cell as described (46). Briefly, RAW 264.7 macrophages were seeded at 5×10^5/ml into 96-well plates in a final volume of 100 μl/well and incubated at 37 °C overnight. The macrophages were infected (MOI 50) with *L. pneumophila* wild type or Δ*icmT* harboring plasmid pSH108 grown for 21 h in AYE supplemented with 0.5 mM isopropyl 1-thio-β-D-galactopyranoside. After 30 min of infection, cells were washed with PBS and lysed with 200 μl of sterile water for 10 min. Lysis was enhanced by shaking the plate on a microplate shaker. Intracellular cAMP was measured by using the cAMP Biotrak enzyme immunoassay system (Amersham Biosciences).

Extracellular Growth Assays—*L. pneumophila* wild type was inoculated with an A_{600} of 0.1 in 200 μl of AYE in 96-well plate format. Three wells were used per sample per test condition. After 12 h of growth at 37 °C and 600 rpm on a temperature-controlled plate shaker (Eppendorf), 10 mM phytate was added for 6 h to one growth set. After an additional 6 h, the bacteria were pelleted for 10 min at 1000 × *g* and carefully suspended in fresh 37 °C AYE medium. Growth on the plate shaker proceeded for another 12 h. A_{600} measurements were taken with a FLUOstar plate reader and subtracted from input values.

Alternatively, *L. pneumophila* wild type, Δ*lppA* mutant, or wild type harboring pRM1 (M45-LppA) was inoculated at an A_{600} of 0.1 in 200 μl of AYE in 96-well plate format. Three wells were used per sample per test condition (0–5 mM phytate). Unused wells were filled with 200 μl of sterile water. Cultures were incubated on a temperature-controlled plate shaker at 24 °C and 600 rpm. Growth was measured after 5 days (A_{600}). Wild type *L. pneumophila* was also grown in 3-ml AYE cultures at 37 °C. Micronutrient supplementation was carried out with $FeN_3O_9 \times 9H_2O$ (Sigma-Aldrich), $ZnCl_2$ (Fluka), $CaCl_2$ (Fluka), or $MgCl_2 \times 6H_2O$ (Fluka). Phytate (final concentration 10 mM) was added to cultures at a ratio of 1:1 with each micronutrient. Cultures were inoculated in triplicate at an A_{600} of 0.1 and allowed to grow for 21 h.

Intracellular Growth Assays and Fluorescence Microscopy—Intracellular growth assays under phytate load were performed with *A. castellanii* or *D. discoideum* amoebae cultured with increasing concentrations of phytate. The compound was added at 2.5 mM, and the concentration was increased every 2 days until the cells were maintained in 10 or 5 mM phytate for *A. castellanii* or *D. discoideum*, respectively. *L. pneumophila* wild type, Δ*icmT*, Δ*lppA* harboring pNT28 (GFP), or Δ*lppA* harboring pWS31 (GFP, LppA) was inoculated in AYE with chloramphenicol (5 μg/ml) and isopropyl 1-thio-β-D-galactopyranoside (1 mM) and grown to early stationary phase. *A. castellanii* or *D. discoideum* was seeded at 5×10^4/well in 200 μl of LoFlo (ForMedium) in a 96-well plate and allowed to adhere for 1 h. Each measured time point of the experiment required one 96-well plate with three allocated wells per strain. *L. pneumophila* cultures were diluted in LoFlo to 2.5×10^4/ml. Medium was removed from adhered cells and replaced with 200 μl of *L. pneumophila* dilutions. Plates were centrifuged at 1,000 × *g* for 5 min and incubated at 37 °C for *A. castellanii* or 23 °C for *D. discoideum*. As an input control, 20 μl of a 1:100 dilution of each strain used for infection was plated onto charcoal yeast extract agar, and colonies were counted after a 3-day incubation at 37 °C.

After centrifugation, one plate for *A. castellanii* ($t = 0$) was imaged by confocal microscopy using a Nikon Eclipse TE300 microscope with a PerkinElmer Life Sciences UltraVIEW spinning disk system and a Hamamatsu Orca Flash 4.0 C-MOS camera. A Nikon 20× Plan Fluor objective was used in combination with filters 488-10BP/525-50BP and bright field. Image evaluation was carried out with Velocity version 6.0.1 software (PerkinElmer Life Sciences). Confocal images of the GFP channel and bright field were captured for each time point.

Quantitative plating assays were performed to complement microscope images because GFP expression could vary between strains. To this end, the infected cells were lysed after microscopic imaging at a given time point, and bacterial dilutions were plated onto charcoal yeast extract agar following the method described previously for colony counting (47). *D. discoideum* amoebae were lysed and plated without imaging. Colony counts for *L. pneumophila* growth in cells not cultured under phytate load followed the same procedure in the absence of phytate supplementation.

Competitive growth in *A. castellanii* between wild type and *lppA* deletion strains was performed as described (47). Finally, the observation of PtdIns(4)P in *D. discoideum* by GFP-$SidC_{P4C}$ was carried out as described previously (21).

Statistical Methods—Differences between *L. pneumophila* strains were evaluated by two-tailed unpaired Student's *t* test assuming unequal variances. Statistical error of the mean is presented as ± one S.D. with 95% confidence intervals.

RESULTS

The Type IV Translocated Cysteine Phosphatase LppA Hydrolyzes Phytate and PIs in Vitro—A PSI-BLAST search using the phosphatase consensus sequence HC*XXGXX*RT identified in the genome of *L. pneumophila* strain Philadelphia-1 (taxid: 272624) a predicted 36.3-kDa protein, Lpg2819, annotated as a putative protein-tyrosine phosphatase II of the DSP superfamily. The only other protein thus identified is annotated as a lysophospholipid acyltransferase. The same search with generic *L. pneumophila* (taxid: 446) yielded results for "protein tyrosine phosphatase" in all sequenced strains. Finally, a search of all available genomes of the family Legionellaceae (taxid: 118969) yielded a hit for at least nine different *Legionella* spp. Lpg2819 is conserved with shared synteny among all *L. pneumophila* strains sequenced thus far (including Philadelphia-1, Paris, Lens, Corby, Alcoy, 130b/AA100, and Lorraine) as well as in *Legionella longbeachae* (64% identity), *L. shakespearei* (64% identity), and *L. dumoffii* (62% identity).

A closer bioinformatic inspection of Lpg2819 revealed an overall similarity to cysteine phytases of *Clostridium* (39% identity), *Stigmatella* (36% identity), *Pseudomonas* (34% identity), and *Xanthomonas* spp. (32% identity) as well as to PhyA from *S. ruminantium* (30% identity) (29, 39, 48) (Fig. 1*A*). The P-loop consensus sequence of *Legionella* spp. is strictly conserved in the phytases from *Clostridium acetobutylicum* and *Stigmatella aurantiaca*. Based on these similarities and the catalytic activities of recombinant Lpg2819 (see below), we termed the protein Lpg2819 "LppA" (*Legionella pneumophila* phytase A).

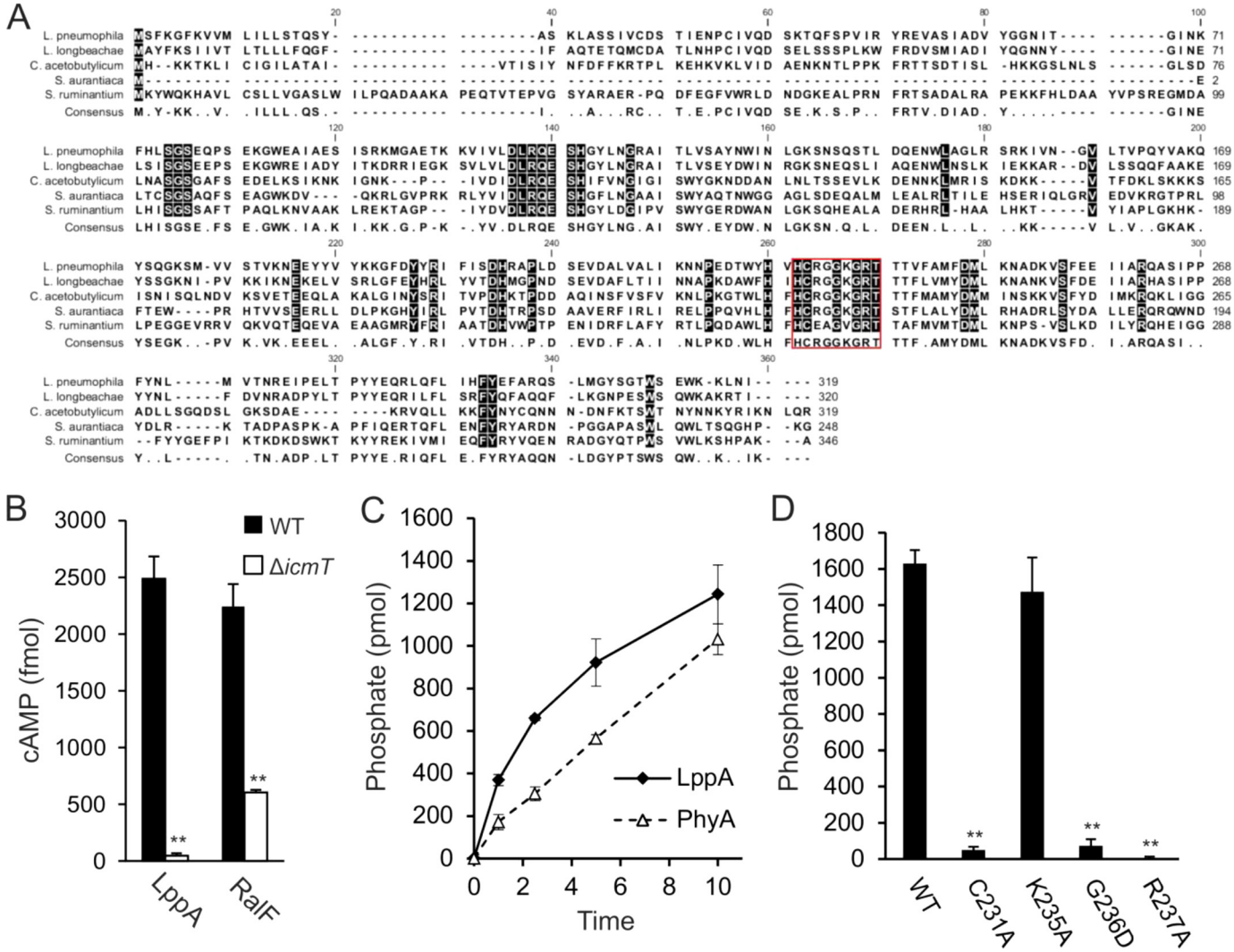

FIGURE 1. **The type IV translocated cysteine phosphatase LppA hydrolyzes phytate *in vitro*.** *A*, alignment of (predicted) cysteine phytases of *L. pneumophila* (LppA), *L. longbeachae*, *S. aurantica*, *C. acetobutylicum*, and *S. ruminantium* (PhyA) in order of decreasing homology to LppA. The *red box* highlights the established or predicted P-loop catalytic active sites for LppA and PhyA as well as for the other putative phytases. *B*, LppA is a substrate of the Icm/Dot T4SS. RAW 264.7 macrophages were infected with wild type or Δ*icmT L. pneumophila* harboring pSH108 (CyaA-LppA) or pSH100 (CyaA-RalF). Levels of cAMP (mean ± S.D. (*error bars*), four duplicate experiments) were measured 30 min postinfection (MOI 50). *C* and *D*, hydrolysis of phytate by GST-LppA$_{\Delta 1-16}$, GST-PhyA$_{\Delta 1-16}$, or GST-LppA$_{\Delta 1-16}$ point mutations of putative catalytically essential residues was measured by phosphate release as a malachite green vanadate dye complex. Reactions proceeded at 25 °C with 2 nmol of phytate and 0.5 μg of protein for up to 10 min (*C*) or 15 min (*D*). Absorbance at 620 nm was measured 20 min after termination of each reaction. The data shown are means and S.D. of triplicates (*B–D*) and are representative of three independent experiments (**, $p < 0.005$).

LppA is not predicted to be translocated and has not been identified as an Icm/Dot T4SS substrate using bioinformatics or experimental approaches (49–52). To determine whether LppA is translocated by the Icm/Dot T4SS, we constructed an N-terminal fusion with the calmodulin-dependent adenylate cyclase CyaA that allows assessment of the production of cAMP upon translocation of the fusion protein to host cell cytoplasm. To this end, RAW 246.7 macrophages were infected with either wild type *L. pneumophila* or the translocation-defective Δ*icmT* mutant strain producing the CyaA-LppA fusion protein (Fig. 1*B*). Calmodulin-dependent production of cAMP was only observed upon infection with wild type *L. pneumophila*; therefore, LppA represents a hitherto unrecognized substrate of the Icm/Dot T4SS. Similarly, the positive control CyaA-RalF was translocated into the host cells in an Icm/Dot-dependent manner. These findings imply that LppA has access to the host cell cytoplasm and performs an intracellular function.

To test potential phytase activity of LppA, we performed a phosphate release assay and compared its activity with that of *S. ruminantium* PhyA. Under the conditions tested, purified GST-LppA hydrolyzed phytate at an initial rate of 5 pmol/s/μg of protein, confirming its activity as an efficient phytase (Fig. 1*C*). The rate of GST-LppA was approximately twice as fast as that of GST-PhyA tested under these conditions. In order to determine the amino acids essential for enzymatic activity, we constructed point mutations in the putative catalytic motif. Mutations of the catalytic residue Cys^{231} or Arg^{237} to Ala resulted in loss of phytase activity (Fig. 1*D*). Moreover, replacing Gly^{236} with a more bulky and charged amino acid, Asp, also abolished phytate hydrolysis, whereas changing Lys^{235} to Ala

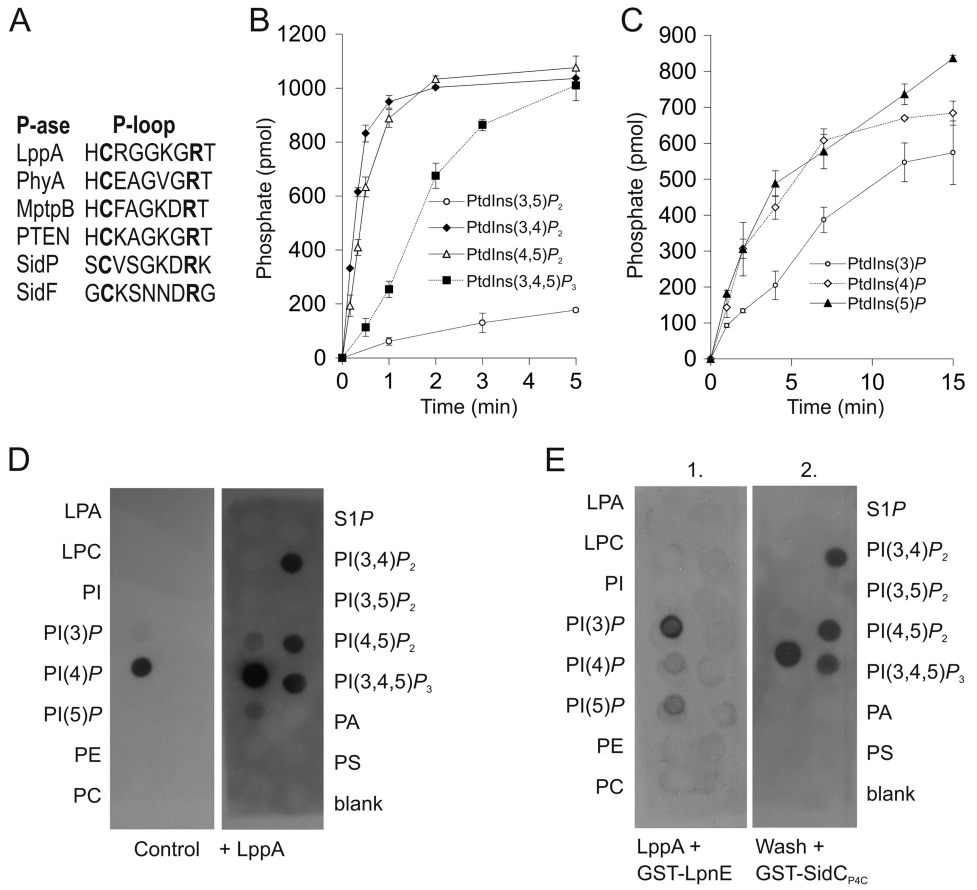

FIGURE 2. **LppA hydrolyzes phosphoinositides and produces PtdIns(4)P *in vitro*.** *A*, alignment of P-loops of bacterial and eukaryotic cysteine phytases and phosphoinositide phosphatases: *L. pneumophila* (*LppA*, *SidF*, and *SidP*), *S. ruminantium* (*PhyA*), *M. tuberculosis* (*MptpB*), and *Homo sapiens* (*PTEN*). *B* and *C*, hydrolysis of PI lipids by $LppA_{\Delta 1-16}$ was measured by phosphate release as a malachite green vanadate dye complex with 1 nmol of dioctyl PI lipids and 0.05 μg (*B*) or 5 μg (*C*) of protein, respectively. *D* and *E*, LppA hydrolyzes polyphosphorylated PIs and produces PtdIns(4)P but not PtdIns(3)P. Nitrocellulose membranes with PI and other lipids (100 pmol/spot) were treated (*right*) or not (*left*) with purified $LppA_{\Delta 1-16}$ (0.5 μg/μl, 10 min) prior to binding of the PtdIns(4)P probe GST-$SidC_{P4C}$ (*D*) or treated with purified $LppA_{\Delta 1-16}$ (0.5 μg/μl, 10 min) and overlaid with the PtdIns(3)P probe GST-LpnE (*left*), followed by washing and overlaying with GST-$SidC_{P4C}$ (*right*) (*E*). Binding was visualized using an anti-GST antibody. *Left lanes* (all membranes), lysophosphatidic acid (*LPA*), lysophosphocholine (*LPC*), PtdIns, phosphoinositide (*PtdIns*(*x*)*P*), phosphatidylethanolamine (*PE*), and phosphatidylcholine (*PC*). *Right lanes* (all membranes), sphingosine 1-phosphate (*S1P*), phosphoinositide, phosphatidic acid (*PA*), and phosphatidylserine (*PS*). The data shown are representative of three independent experiments. *Error bars*, S.D.

did not alter the activity. Taken together, *L. pneumophila* produces a translocated cysteine phosphatase that *in vitro* shows a 2-fold higher phytase activity than PhyA and harbors the conserved amino acids Cys^{215} and Arg^{221} implicated in catalysis.

LppA Hydrolyzes Phosphoinositides in Vitro and Produces PtdIns(4)P—Given that inositol phosphates make up the identity-defining headgroup of PI lipids, we tested whether these derivatives of phytate could be metabolized by LppA *in vitro*. The P-loop consensus sequence of the *L. pneumophila* phytase is similar to those of the mammalian and bacterial PI phosphatases (Fig. 2*A*). In fact, the catalytically active site of LppA (HCRGGKGRT) is almost identical to the human PI 3-phosphatase PTEN (HCR/KAGKGRT) and very similar to the mycobacterial PI phosphatase MptpB (HCFAGKDRT). Therefore, we also tested the putative PI phosphatase activity of the enzyme toward dioctyl-PI lipids. LppA dephosphorylated the diphosphorylated PIs PtdIns(3,4)P_2 and PtdIns(4,5)P_2 very efficiently, followed by PtdIns(3,4,5)P_3 as a substrate and, with ~20 times lower activity, PtdIns(3,5)P_2 (Fig. 2*B*). A 100-fold higher amount of enzyme was required to observe poor activity toward monophosphorylated PIs (Fig. 2*C*).

To analyze the PI product(s) generated by LppA *in vitro*, we treated nitrocellulose membranes spotted with all seven PIs and other lipids with the enzyme and subsequently performed a protein-lipid overlay using the PtdIns(4)P-specific probe GST-$SidC_{P4C}$ (Fig. 2*D*). GST-$SidC_{P4C}$ bound on untreated control membranes exclusively to the PtdIns(4)P spot as described previously (18). In contrast, on membranes pretreated with LppA, GST-$SidC_{P4C}$ also bound to the spots initially occupied by PtdIns(3,4)P_2, PtdIns(4,5)P_2, or PtdIns(3,4,5)P_3, indicating that PtdIns(4)P is the major PI product of the phosphatase. In parallel, the LppA-treated membrane was probed with GST-LpnE to detect PtdIns(3)P, yet the fusion protein bound only to the initial PtdIns(3)P spot, indicating that no PtdIns(3)P was produced by the phosphatase LppA (Fig. 2*E*). Thus, *in vitro* LppA also rapidly metabolizes polyphosphorylated PI lipids containing a 4-phosphate residue to yield PtdIns(4)P.

High Resolution Structure of L. pneumophila LppA—Toward understanding LppA function at the molecular level, we determined the crystal structure of the phytase apo-form by molecular replacement at 1.4 Å resolution. The data collec-

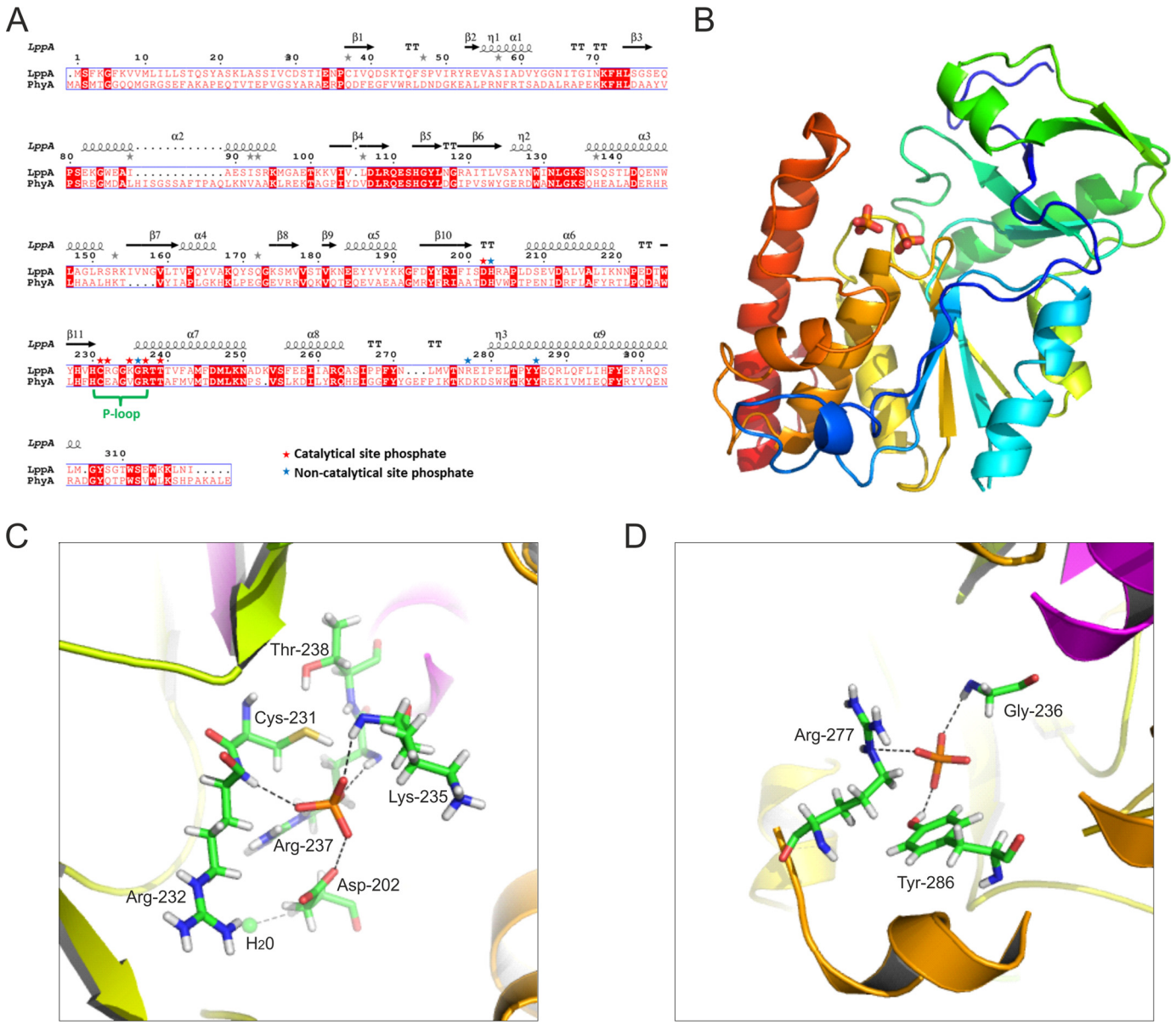

FIGURE 3. **Overall structure of *L. pneumophila* LppA binding two phosphates.** *A*, structure-based alignment of *L. pneumophila* LppA with *S. ruminantium* PhyA. *B*, overall structure of LppA showing two bound phosphates (phosphorus (*orange*) and oxygen (*red*)). *C*, *close-up view* of the catalytic P-loop site of LppA coordinating a phosphate with the amino acids Asp^{202}, Cys^{231}, Arg^{232}, Lys^{235}, Arg^{237}, and Thr^{238}. *D*, *close-up view* of the second phosphate coordinated at a non-catalytic site by Gly^{236}, Arg^{277}, and Tyr^{286}.

tion and refinement statistics are listed in Table 3, and a structure-based alignment of LppA with PhyA is shown in Fig. 3*A*. The current model of LppA consists of amino acid residues 26–314 (chain B in the unit cell tetramer) and reveals an overall structure of a mainly α-helical globular protein stabilized by four antiparallel β-sheets (Fig. 3*B*). The catalytic site forms a PTP-like fold characteristic of dual specificity Ser/Thr and Tyr protein phosphatases.

One remarkable feature of the LppA crystal structure is the binding of two phosphate moieties in a positively charged pocket formed by the basic amino acids His^{203}, Arg^{232}, Lys^{235}, Arg^{237}, and Arg^{277}. This pocket probably accommodates the binding sites for two of the six phosphate residues of phytate. One phosphate localizes to the active site P-loop and is coordinated by the amino acids Cys^{231}, Arg^{232}, Lys^{235}, and Arg^{237} (Fig. 3*C*). The position of Cys^{231} suggests a catalytic mechanism, where the thiolate anion of Cys^{231} is the nucleophile that attacks a phytate phosphate to form a cysteinyl-phosphate trigonal-bipyramidal pentavalent intermediate. The negative charge on the Sγ atom of Cys^{231} might be stabilized by the hydroxyl group of the conserved adjacent Thr^{238} (Fig. 2*A*). Also located in the catalytic pocket, Asp^{202} probably acts as a general acid and donates a proton to form *myo*-inositol pentakisphosphate. In the second step of the phosphatase reaction, Asp^{202} might act as a general base accepting a proton from a nearby water molecule (at a distance of 3.4 Å), which upon nucleophilic attack liberates phosphate and regenerates the active cysteinyl-phosphatase.

The second phosphate, which cannot be directly hydrolyzed, is coordinated by Gly^{236}, Arg^{277}, and Tyr^{286} and is further sta-

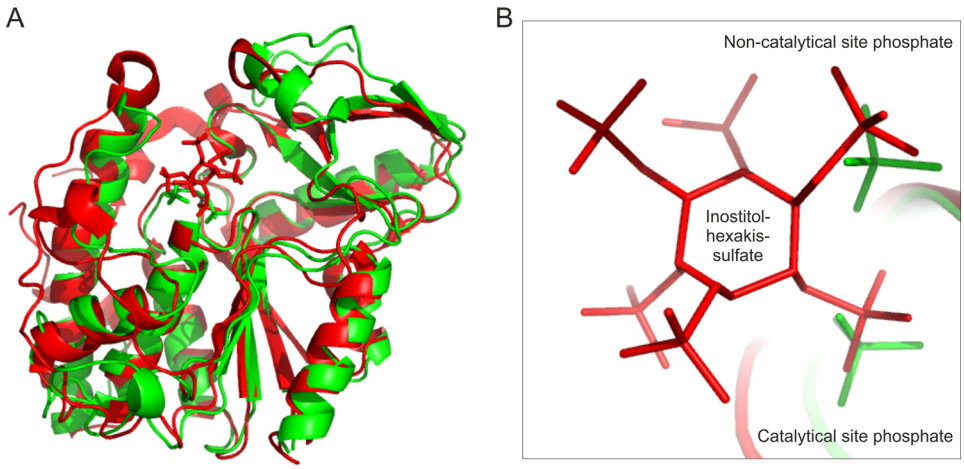

FIGURE 4. **Comparison of overall structure and active sites of *L. pneumophila* LppA and *S. ruminantium* PhyA.** *A*, overlay of the overall structures; *B*, *close-up view* of the catalytic P-loop sites of *L. pneumophila* LppA (*green*) and *S. ruminantium* PhyA (*red*) binding two phosphates (*green*) or the inhibitor *myo*-inositol hexasulfate (*IHS*; *red*), respectively.

bilized by His^{203} and the neighboring phosphate (Fig. 3*D*). The arrangement of the two adjacent phosphate moieties bound to LppA is in agreement with a model proposed for the phytase PhyA from *S. ruminantium*, suggesting that after hydrolytic removal of the first phosphate, *myo*-inositol pentakisphosphate rotates, and a second phosphate is placed in the vicinity of the catalytically active cysteine to be subsequently hydrolyzed in a stepwise manner (39).

Comparison of L. pneumophila LppA and S. ruminantium PhyA—The phytase LppA is structurally similar to the *S. ruminantium* phytase PhyA in its apo-form (Protein Data Bank code 1U24). C_α superimposition of PhyA onto LppA results in a root mean square deviation of 1.6 Å over 254 residues and 28% sequence identity (Fig. 4*A*). Significant differences in structure are seen at the N and C termini that extend by 11 and 9 residues in PhyA, respectively. Furthermore, LppA is lacking a loop present in PhyA (amino acids 88–99). These results are in good agreement with the overall similarity of LppA and PhyA, which share 30% sequence identity.

The P-loop sites of LppA (HCRGGKGRT) and PhyA (HCEAGVGRT) are 66% identical, and the phosphate groups bound by LppA superimposes with S4 and S5 of the inhibitor *myo*-inositol hexasulfate (*IHS*) that was co-crystallized with PhyA from *S. ruminantium* (PDB code 1U26) (Fig. 4*B*). It is noteworthy that Arg^{232} and Arg^{277}, coordinating in LppA the phosphate residues in the catalytic or the non-catalytic site, respectively, are replaced by acidic amino acids in PhyA (Glu^{242} and Asp^{289}). Moreover, LppA Lys^{235} is not conserved in PhyA, and accordingly, its replacement by Ala did not affect the catalytic activity of LppA (Fig. 1*D*). In contrast, mutation of PhyA His^{213} or Tyr^{298}, which form the substrate-binding pocket and are conserved in LppA (His^{187} and Tyr^{270}), caused a significant decrease in phytase activity by 52 and 92%, respectively (39). In summary, these findings suggest a similar mechanism of phytate binding and catalysis of LppA and PhyA.

Phytate Reversibly Inhibits L. pneumophila Growth and Is Counteracted by LppA or Micronutrient Supplementation—To investigate the effect of phytate on the growth of *L. pneumophila* in AYE broth, the compound was added to a bacterial culture in early exponential growth phase (Fig. 5*A*). Under these conditions, 10 mM phytate caused growth stasis of *L. pneumophila*. The bacteria were subsequently pelleted, suspended in fresh AYE medium, and allowed to grow again. After phytate was removed, *L. pneumophila* resumed growth at the initial rate. Therefore, phytate is not toxic to *L. pneumophila* but reversibly inhibits growth of the bacteria and thus exerts a bacteriostatic rather than a bactericidal effect.

Next, we thought to assess the effect of LppA on growth inhibition by phytate. To this end, an *L. pneumophila* mutant strain lacking *lppA* (Δ*lppA*) was generated by double homologous recombination. Western blots using a polyclonal anti-LppA antibody revealed that the Δ*lppA* mutant strain did not produce LppA anymore, yet phytase production was restored upon expression of plasmid-encoded *lppA* (pWS31) (Fig. 5*B*) (data not shown). Moreover, upon overproduction of LppA by wild type *L. pneumophila*, some phytase was detected in the supernatants of bacterial cultures. Growth of *L. pneumophila* wild type, Δ*lppA*, or wild type overproducing LppA in AYE medium supplemented with 0–5 mM phytate was monitored by measuring the optical density of the culture. In the absence of phytate, the *L. pneumophila* strains grew indistinguishably. The addition of phytate inhibited bacterial growth in a dose-dependent manner, and a 5 mM concentration of the compound completely abolished bacterial replication (Fig. 5*C*). *L. pneumophila* lacking *lppA* was slightly more susceptible to phytate upon growth at 24 °C but not at 37 °C, regardless of whether complex AYE or chemically defined minimal medium was used (data not shown). On the other hand, the wild type strain overproducing LppA grew significantly better at phytate concentrations ranging from 1 to 4 mM. Thus, LppA phytase (released from the bacteria) counteracts the bacteriostatic effect of phytate (Fig. 5, *B* and *C*).

Phytate is a strong chelator and complexes iron, calcium, zinc, and magnesium among other micronutrients (37). In order to test whether the bacteriostatic effect of phytate on *L. pneumophila* is due to its chelating properties, we added the compound in the presence of equimolar concentrations of micronutrients (iron, zinc, magnesium, or calcium) to bacterial

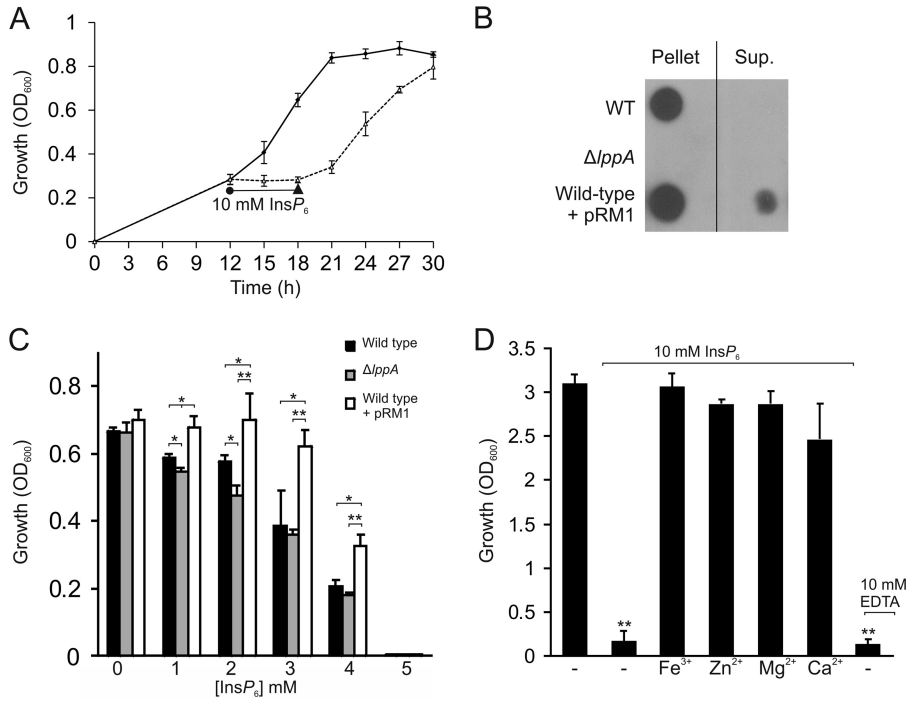

FIGURE 5. **Phytate reversibly inhibits *L. pneumophila* growth and is counteracted by LppA or micronutrient supplementation.** *A*, phytate is bacteriostatic for *L. pneumophila*. Wild type *L. pneumophila* was inoculated at an A_{600} of 0.1 in AYE medium, and growth was measured by A_{600} every 3 h from 12 to 30 h. At 12 h, 10 mM phytate (*InsP_6*) was added for 6 h (*dashed line*), and the bacteria were pelleted, resuspended in fresh AYE medium, and allowed to grow again. The control without phytate was treated the same way. *B*, detection of LppA by Western blot in *L. pneumophila* wild type or Δ*lppA* harboring pCR33 (vector), wild type harboring pRM1 (M45-LppA), and culture supernatants. The data shown are representative of two independent experiments. *C*, growth inhibition by phytate is counteracted by LppA. *L. pneumophila* wild type or Δ*lppA* harboring pCR33 (vector) or wild type harboring pRM1 (M45-LppA) was grown in AYE supplemented with 0–5 mM phytate for 5 days at 24 °C. *D*, micronutrient supplementation of *L. pneumophila* cultures grown with 10 mM phytate. *L. pneumophila* was grown for 21 h in AYE containing 10 mM phytate or 10 mM of the micronutrients indicated (iron, zinc, magnesium, or calcium). 10 mM EDTA alone was used as a control for chelation. Data (*A–C*) represent means ± S.D. (*error bars*) of triplicates (*, $p < 0.05$; **, $p < 0.005$).

cultures growing in AYE medium and assessed growth. Whereas 10 mM phytate (or the positive control EDTA) completely blocked the growth of *L. pneumophila*, the concomitant addition of 10 mM micronutrients reversed the inhibition (Fig. 5*D*). In summary, supplementation of phytate with equimolar concentrations of metal ions reversed the bacteriostatic effects of phytate; therefore, growth inhibition is due to micronutrient deprivation by the chelator.

LppA Promotes Intracellular Replication of L. pneumophila in Phytate-loaded Amoebae—To determine whether phytate plays a role in intracellular replication of *L. pneumophila*, we preloaded *A. castellanii* or *D. discoideum* with the chelator. To this end, the amoebae were initially treated with 2.5 mM phytate, and the concentration was increased every 2 days up to 10 mM for *A. castellanii* or 5 mM for *D. discoideum*. Shortly before an experiment, the amoebae were washed and suspended in LoFlo medium. The phytate-loaded amoebae were then infected with GFP-producing *L. pneumophila* wild type, Δ*icmT*, Δ*lppA*, or complemented Δ*lppA* strains. Bright field and GFP fluorescence microscopy images were taken for infected *A. castellanii*.

Images immediately following infection show an even distribution of amoebae and *L. pneumophila* (Fig. 6*A*). After 48 h, amoebae infected with wild type *L. pneumophila* or the complemented Δ*lppA* mutant strain predominantly had rounded up, which is a characteristic of advanced *L. pneumophila* infection. The bright field channel shows that the majority of the cells are filled with bacteria, many of which are producing GFP. The synthesis of GFP was rather low and heterogeneous for the complementation strain, producing a short lived GFP. In contrast, amoebae infected with *L. pneumophila* lacking *lppA* remained largely attached, the morphology of most amoebae was similar to cells infected with Δ*icmT*, and only a few amoebae were observably filled with bacteria. By 72 h postinfection, *A. castellanii* infected with wild type *L. pneumophila* were full of actively moving bacteria ready for exit (supplemental Movie S1), and many amoebae infected with the complemented Δ*lppA* mutant strain had burst, releasing the intracellular bacteria (supplemental Movie S2). Replication of the Δ*lppA* mutant strain increased over the 48 h time point but was still considerably lower than replication by wild type or complementation strains (supplemental Movie S3), and many cells resembled the Δ*icmT*-infected amoebae (supplemental Movie S4).

Intracellular growth of the *L. pneumophila* strains in phytate-loaded *A. castellanii* or *D. discoideum* was also quantified by determining cfu (Fig. 6, *B* and *C*). Colony counts at the onset of infection were even across all strains, and Δ*icmT* mutant bacteria used as a negative control disappeared over time. Using cfu as readout for intracellular replication, significantly fewer bacteria lacking *lppA* were counted after 48 or 72 h of infection, and the growth defect was fully complemented by providing the gene on a plasmid.

We also tested the possible role of *lppA* in intracellular growth of *L. pneumophila* in *A. castellanii* or *D. discoideum* cultured in the absence of phytate. To this end, the amoebae

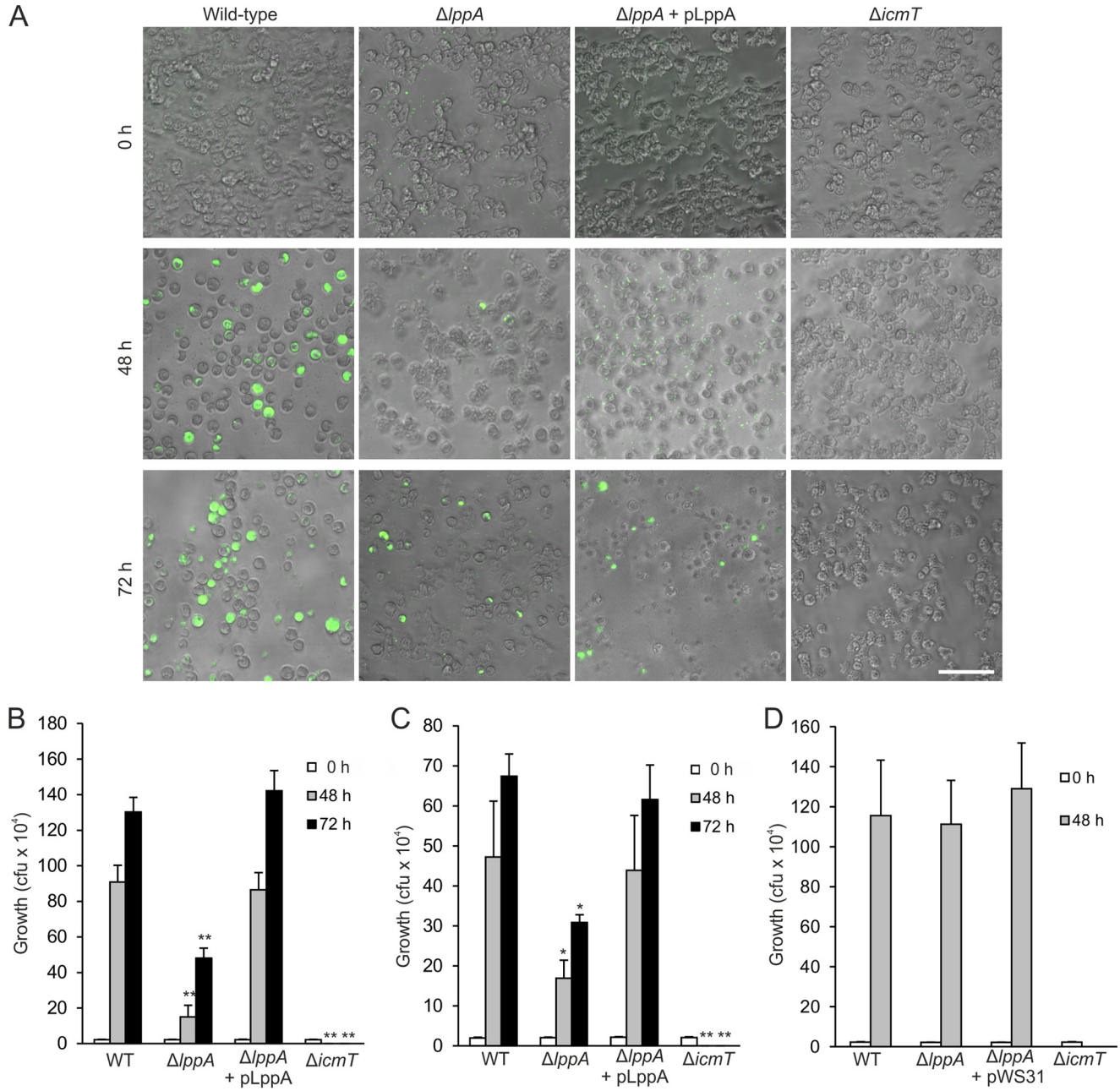

FIGURE 6. **LppA promotes intracellular replication of *L. pneumophila* under phytate load.** *A*, *A. castellanii* amoebae cultured in the presence of 10 mM phytate were infected (MOI 1, 37 °C) with *L. pneumophila* wild type, Δ*lppA*, or Δ*icmT* harboring pNT28 (GFP) or Δ*lppA* harboring pWS31 (GFP and LppA). Shown are bright field and GFP fluorescence images for infected *A. castellanii* taken at 0, 48, or 72 h postinfection. Scale bar, 50 μm. *B*, cfu counts for intracellular replication of *L. pneumophila* strains corresponding to images in (*A*). *C*, cfu counts for intracellular replication of above-listed *L. pneumophila* strains at 23 °C in *D. discoideum* preloaded with 5 mM phytate. Data represent means ± S.D. (*error bars*) of triplicates and are representative of three independent experiments (*, $p < 0.05$; **, $p < 0.005$). *D*, *A. castellanii* cultured in the absence of phytate was infected (MOI 1, 37 °C) with *L. pneumophila* wild type, Δ*lppA* or Δ*icmT* harboring pNT28 (GFP), or Δ*lppA* harboring pWS31 (GFP and LppA), and intracellular growth was determined by cfu at 0 and 48 h postinfection.

were grown in standard medium and infected with *L. pneumophila* wild type, Δ*icmT*, Δ*lppA*, or complemented Δ*lppA* strains, and intracellular growth was determined by cfu after 48 h infection. However, under these conditions, the deletion or overexpression of *lppA* did not affect intracellular bacterial growth (Fig. 6*D*) (data not shown). Moreover, upon co-infection of *A. castellanii* with *L. pneumophila* wild type and Δ*lppA* at a 1:1 ratio, the mutant strain was not outcompeted for up to 18 days (data not shown). Finally, *lppA* did not affect the growth of *L. pneumophila* in RAW 264.7 macrophages, for which phytate was toxic (data not shown). In summary, these findings indicated that the *L. pneumophila* translocated phytase LppA provides an intracellular growth advantage in phytate-loaded amoebae, such as *A. castellanii* or *D. discoideum*.

LppA Does Not Play a Major Role in the Modulation of the LCV PI Pattern—LppA is translocated into host cells and *in vitro* efficiently hydrolyzes PI lipids to yield PtdIns(4)P (Fig. 2). Thus, we hypothesized that LppA might also modulate the LCV PI pattern in *L. pneumophila*-infected cells. To compare the dynamics of PtdIns(4)P accumulation on LCVs harboring wild

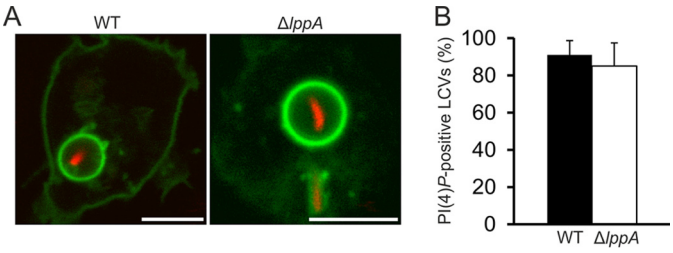

FIGURE 7. **LppA does not influence the LCV PtdIns(4)P pattern in infected phagocytes.** *A*, live cell imaging of *D. discoideum* producing GFP-SidC$_{P4C}$ infected with *L. pneumophila* wild-type or Δ*lppA* harboring pSW001 (DsRed) at MOI 10. Images were taken 2 h postinfection at 23 °C. *Scale bars*, 5 μm. *B*, quantification of PtdIns(4)P-positive LCVs. At least 100 LCVs were counted for each sample 2 h postinfection. *Scale bar*, 5 μm. *Error bars*, S.D.

type or Δ*lppA* mutant bacteria, we performed live cell imaging using specific PI probes (21). Upon infection of *D. discoideum* amoebae producing GFP-SidC$_{P4C}$ with *L. pneumophila*, LCVs harboring wild type or Δ*lppA* bacteria accumulated PtdIns(4)P to the same extent within 1 or 2 h postinfection (Fig. 7, *A* and *B*). The LCVs were similar in size and GFP-SidC$_{P4C}$ signal intensity, and PtdIns(4)P persisted on LCVs containing replicating bacteria. Similar results were obtained upon staining the endogenously produced PtdIns(4)P-binding effector SidC on LCVs harboring wild type or Δ*lppA L. pneumophila* (data not shown). Finally, LCVs harboring *L. pneumophila* wild type or Δ*lppA* mutant bacteria were decorated to the same extent with the ER marker calnexin (data not shown). Taken together, the translocated *L. pneumophila* phytase LppA does not appear to modulate the LCV PI pattern in infected cells.

DISCUSSION

In this study, we identified the chelator phytate as an intracellular bacteriostatic compound, and we provide evidence that the T4SS-translocated *L. pneumophila* phytase LppA counteracts bacterial growth restriction by phytate by hydrolyzing and thus inactivating the chelator. *L. pneumophila* requires iron for growth (53), and accordingly, the standard AYE growth medium contains 0.6 mM iron. The bacteria possess a number of iron uptake systems, including the siderophore legiobactin and the ferrous iron transmembrane transporter FeoB (54). The requirement for iron and possibly other micronutrients provides a rationale for the susceptibility of *L. pneumophila* to the chelator phytate (Fig. 5). The sensitivity of *L. pneumophila* to phytate also suggests that under the conditions tested, the bacteria do not use phytate as a source of phosphorus or as a siderophore for micronutrients, which has been described for *X. oryzae* (34) or *P. aeruginosa* (35, 36), respectively.

Upon extracellular growth in AYE broth, an *L. pneumophila* strain lacking *lppA* was only slightly more susceptible to phytate. The mild phenotype was observed only at a low growth temperature of 24 °C and not at 37 °C, regardless of whether complex AYE or chemically defined minimal medium was used (data not shown). In contrast, the wild type strain overproducing LppA grew significantly better in the presence of 1–4 mM phytate (Fig. 5*C*). The overproduction of LppA resulted in a portion of the phytase being released by the bacteria (Fig. 5*B*). Therefore, these findings are in agreement with the notion that LppA in the growth medium counteracts the bacteriostatic effect of phytate. The polyanionic compound phytate is expected to be largely membrane-impermeable and might not be taken up actively by *L. pneumophila*. Hence, under extracellular conditions where LppA is not translocated into a host cell, the absence of the phytase does not result in a pronounced growth defect.

Amoebae, in particular the social soil amoeba *D. discoideum*, produce phytate in the millimolar range (31–33). Phytate concentrations above 1–2 mM inhibit the extracellular growth of *L. pneumophila* (Fig. 5*C*), very likely due to the chelation of micronutrients (Fig. 5*D*). It is challenging to quantify the intracellular concentrations of micronutrients and the intracellular micronutrient requirements of *L. pneumophila* in host cells, yet the intracellular production of phytate in millimolar quantities seems sufficient to reduce or even deplete from pathogen-accessible intracellular compartments the micronutrients essential for *L. pneumophila*. We showed that *D. discoideum* as well as *A. castellanii* preloaded with phytate (but not amoebae grown in standard media) restrict intracellular growth of *L. pneumophila* in an *lppA*-dependent manner (Fig. 6). Perhaps the micronutrients available under the laboratory conditions used overcompensated the endogenous phytate produced by the amoeba.

Protozoa take up solutes via macropinocytic processes, and the macropinosomes formed probably communicate with LCVs. In support of this notion, *L. pneumophila* itself is taken up by phagocytes by macropinocytic rather than phagocytic processes (21, 55). Thus, the exogenously added phytate might reach the pathogen compartment through vesicle fusion, yet transmembrane transport processes might also play a role. Notably, the obligate intra-amoebal bacterium *Candidatus Protochlamydia amoebophila*, produces a putative cysteine phytase (32% identity with LppA) (29). This finding suggests that the phytate-containing compartment communicates with the bacterial symbiont and that degradation of intracellular phytate might also be beneficial for survival and replication of this bacterium.

Although LppA hydrolyzes phytate as well as polyphosphorylated PI lipids *in vitro*, only the phytase activity appears to be relevant in infected cells (Figs. 6 and 7). Other *L. pneumophila* Icm/Dot substrates, such as the PI phosphatases SidF and SidP, as well as host PI-metabolizing enzymes seem to modulate and define the LCV PI pattern. This is consistent with the notion that LppA apparently plays only a minor if any role in LCV formation. Cysteine phytases are characterized by the catalytic motif HCX_2GX_2R, of which the Cys and Arg residues are catalytically essential and His and Gly are important for conformation of the P-loop (39). Whereas the catalytic motif of LppA (HCRGGKGRT) is 66% identical to PhyA (HCEAGVGRT), it shares 89% identity with the mammalian PI 3-phosphatase PTEN (HC(R/K)AGKGRT) (Fig. 2*A*). Because both PTEN and LppA (Fig. 2*B*) effectively metabolize PtdIns(3,4,5)P_3 and the main PI product of LppA *in vitro* is PtdIns(4)P (Fig. 2, *D* and *E*), it is tantalizing that LppA apparently does not function as a PI phosphatase in infected cells.

The results obtained in this study emphasize the critical role of micronutrients for intracellular pathogens. As an antibacterial strategy against vacuolar pathogens, micronutrient deple-

tion by the chelator phytate might function in parallel with transporters that remove metal ions from the pathogen vacuole. Accordingly, the transmembrane proteins Nramp-1 and Nramp-2 have been shown to pump iron from vacuoles (LCVs) to the cytoplasm of *D. discoideum* (56, 57). Whereas the eukaryotic cell limits the availability of micronutrients by producing chelators and ion pumps, the intracellular pathogen *L. pneumophila* developed means to counteract the bacteriostatic strategy. Thus, our study reveals the potential to exploit intracellular micronutrient deprivation as an antibacterial strategy. Specifically, phytases or other microbial chelator antagonists might represent targets to control intracellular growth and virulence of bacterial pathogens.

Acknowledgments—We thank Aline Kessler and Sabrina Heiny for constructing pAK7 and pSH108, respectively.

REFERENCES

1. Newton, H. J., Ang, D. K., van Driel, I. R., and Hartland, E. L. (2010) Molecular pathogenesis of infections caused by *Legionella pneumophila*. *Clin. Microbiol. Rev.* **23,** 274–298
2. Hilbi, H., Hoffmann, C., and Harrison, C. F. (2011) *Legionella* spp. outdoors: colonization, communication and persistence. *Environ. Microbiol. Rep.* **3,** 286–296
3. Whiley, H., and Bentham, R. (2011) *Legionella longbeachae* and legionellosis. *Emerg. Infect. Dis.* **17,** 579–583
4. Hoffmann, C., Harrison, C. F., and Hilbi, H. (2014) The natural alternative: protozoa as cellular models for *Legionella* infection. *Cell Microbiol.* **16,** 15–26
5. Isberg, R. R., O'Connor, T. J., and Heidtman, M. (2009) The *Legionella pneumophila* replication vacuole: making a cosy niche inside host cells. *Nat. Rev. Microbiol.* **7,** 13–24
6. Hubber, A., and Roy, C. R. (2010) Modulation of host cell function by *Legionella pneumophila* type IV effectors. *Annu. Rev. Cell Dev. Biol.* **26,** 261–283
7. Hilbi, H., and Haas, A. (2012) Secretive bacterial pathogens and the secretory pathway. *Traffic* **13,** 1187–1197
8. Itzen, A., and Goody, R. S. (2011) Covalent coercion by *Legionella pneumophila*. *Cell Host. Microbe* **10,** 89–91
9. Sherwood, R. K., and Roy, C. R. (2013) A Rab-centric perspective of bacterial pathogen-occupied vacuoles. *Cell Host. Microbe* **14,** 256–268
10. Rothmeier, E., Pfaffinger, G., Hoffmann, C., Harrison, C. F., Grabmayr, H., Repnik, U., Hannemann, M., Wölke, S., Bausch, A., Griffiths, G., Müller-Taubenberger, A., Itzen, A., and Hilbi, H. (2013) Activation of Ran GTPase by a *Legionella* effector promotes microtubule polymerization, pathogen vacuole motility and infection. *PLoS Pathog.* **9,** e1003598
11. Hoffmann, C., Finsel, I., Otto, A., Pfaffinger, G., Rothmeier, E., Hecker, M., Becher, D., and Hilbi, H. (2014) Functional analysis of novel Rab GTPases identified in the proteome of purified *Legionella*-containing vacuoles from macrophages. *Cell Microbiol.* **16,** 1034–1052
12. Simon, S., Wagner, M. A., Rothmeier, E., Müller-Taubenberger, A., and Hilbi, H. (2014) Icm/Dot-dependent inhibition of phagocyte migration by *Legionella* is antagonized by a translocated Ran GTPase activator. *Cell Microbiol.* **16,** 977–992
13. Hilbi, H., Rothmeier, E., Hoffmann, C., and Harrison, C. F. (2014) Beyond Rab GTPases: *Legionella* activates the small GTPase Ran to promote microtubule polymerization, pathogen vacuole motility, and infection. *Small GTPases,* in press
14. Ham, H., Sreelatha, A., and Orth, K. (2011) Manipulation of host membranes by bacterial effectors. *Nat. Rev. Microbiol.* **9,** 635–646
15. Hilbi, H., Weber, S., and Finsel, I. (2011) Anchors for effectors: subversion of phosphoinositide lipids by *Legionella*. *Front. Microbiol.* **2,** 91
16. Haneburger, I., and Hilbi, H. (2013) Phosphoinositide lipids and the *Legionella* pathogen vacuole. *Curr. Top. Microbiol. Immunol.* **376,** 155–173
17. Weber, S. S., Ragaz, C., Reus, K., Nyfeler, Y., and Hilbi, H. (2006) *Legionella pneumophila* exploits PI(4)P to anchor secreted effector proteins to the replicative vacuole. *PLoS Pathog.* **2,** e46
18. Ragaz, C., Pietsch, H., Urwyler, S., Tiaden, A., Weber, S. S., and Hilbi, H. (2008) The *Legionella pneumophila* phosphatidylinositol-4-phosphate-binding type IV substrate SidC recruits endoplasmic reticulum vesicles to a replication-permissive vacuole. *Cell Microbiol.* **10,** 2416–2433
19. Brombacher, E., Urwyler, S., Ragaz, C., Weber, S. S., Kami, K., Overduin, M., and Hilbi, H. (2009) Rab1 guanine nucleotide exchange factor SidM is a major phosphatidylinositol 4-phosphate-binding effector protein of *Legionella pneumophila*. *J. Biol. Chem.* **284,** 4846–4856
20. Schoebel, S., Blankenfeldt, W., Goody, R. S., and Itzen, A. (2010) High-affinity binding of phosphatidylinositol 4-phosphate by *Legionella pneumophila* DrrA. *EMBO Rep.* **11,** 598–604
21. Weber, S., Wagner, M., and Hilbi, H. (2014) Live cell imaging of phosphoinositide dynamics and membrane architecture during *Legionella* infection. *mBio* **5,** e00839-13
22. Dolinsky, S., Haneburger, I., Cichy, A., Hannemann, M., Itzen, A., and Hilbi, H. (2014) The *Legionella longbeachae* Icm/Dot substrate SidC selectively binds PtdIns(4)P with nanomolar affinity and promotes pathogen vacuole-ER interactions. *Infect Immun.* **82,** 4021–4033
23. Weber, S. S., Ragaz, C., and Hilbi, H. (2009) The inositol polyphosphate 5-phosphatase OCRL1 restricts intracellular growth of *Legionella*, localizes to the replicative vacuole and binds to the bacterial effector LpnE. *Cell Microbiol.* **11,** 442–460
24. Jank, T., Böhmer, K. E., Tzivelekidis, T., Schwan, C., Belyi, Y., and Aktories, K. (2012) Domain organization of *Legionella* effector SetA. *Cell Microbiol.* **14,** 852–868
25. Finsel, I., Ragaz, C., Hoffmann, C., Harrison, C. F., Weber, S., van Rahden, V. A., Johannes, L., and Hilbi, H. (2013) The *Legionella* effector RidL inhibits retrograde trafficking to promote intracellular replication. *Cell Host Microbe* **14,** 38–50
26. Hsu, F., Zhu, W., Brennan, L., Tao, L., Luo, Z. Q., and Mao, Y. (2012) Structural basis for substrate recognition by a unique *Legionella* phosphoinositide phosphatase. *Proc. Natl. Acad. Sci. U.S.A.* **109,** 13567–13572
27. Toulabi, L., Wu, X., Cheng, Y., and Mao, Y. (2013) Identification and structural characterization of a *Legionella* phosphoinositide phosphatase. *J. Biol. Chem.* **288,** 24518–24527
28. Turner, B. L., Papházy, M. J., Haygarth, P. M., and McKelvie, I. D. (2002) Inositol phosphates in the environment. *Philos. Trans. R. Soc. Lond. B Biol. Sci.* **357,** 449–469
29. Lim, B. L., Yeung, P., Cheng, C., and Hill, J. E. (2007) Distribution and diversity of phytate-mineralizing bacteria. *ISME J.* **1,** 321–330
30. Rao, D. E., Rao, K. V., Reddy, T. P., and Reddy, V. D. (2009) Molecular characterization, physicochemical properties, known and potential applications of phytases: an overview. *Crit. Rev. Biotechnol.* **29,** 182–198
31. Martin, J. B., Foray, M. F., Klein, G., and Satre, M. (1987) Identification of inositol hexaphosphate in ^{31}P-NMR spectra of *Dictyostelium discoideum* amoebae. Relevance to intracellular pH determination. *Biochim. Biophys. Acta* **931,** 16–25
32. Stephens, L. R., and Irvine, R. F. (1990) Stepwise phosphorylation of *myo*-inositol leading to *myo*-inositol hexakisphosphate in *Dictyostelium*. *Nature* **346,** 580–583
33. Pisani, F., Livermore, T., Rose, G., Chubb, J. R., Gaspari, M., and Saiardi, A. (2014) Analysis of *Dictyostelium discoideum* inositol pyrophosphate metabolism by gel electrophoresis. *PLoS One* **9,** e85533
34. Chatterjee, S., Sankaranarayanan, R., and Sonti, R. V. (2003) PhyA, a secreted protein of *Xanthomonas oryzae* pv. *oryzae*, is required for optimum virulence and growth on phytic acid as a sole phosphate source. *Mol. Plant Microbe Interact.* **16,** 973–982
35. Smith, A. W., Poyner, D. R., Hughes, H. K., and Lambert, P. A. (1994) Siderophore activity of *myo*-inositol hexakisphosphate in *Pseudomonas aeruginosa*. *J. Bacteriol.* **176,** 3455–3459
36. Hirst, P. H., Riley, A. M., Mills, S. J., Spiers, I. D., Poyner, D. R., Freeman, S., Potter, B. V., and Smith, A. W. (1999) Inositol polyphosphate-mediated iron transport in *Pseudomonas aeruginosa*. *J. Appl. Microbiol.* **86,** 537–543
37. Urbano, G., López-Jurado, M., Aranda, P., Vidal-Valverde, C., Tenorio, E.,

and Porres, J. (2000) The role of phytic acid in legumes: antinutrient or beneficial function? *J. Physiol. Biochem.* **56,** 283–294
38. Mullaney, E. J., and Ullah, A. H. (2003) The term phytase comprises several different classes of enzymes. *Biochem. Biophys. Res. Commun.* **312,** 179–184
39. Chu, H. M., Guo, R. T., Lin, T. W., Chou, C. C., Shr, H. L., Lai, H. L., Tang, T. Y., Cheng, K. J., Selinger, B. L., and Wang, A. H. (2004) Structures of *Selenomonas ruminantium* phytase in complex with persulfated phytate: DSP phytase fold and mechanism for sequential substrate hydrolysis. *Structure* **12,** 2015–2024
40. Norris, F. A., Wilson, M. P., Wallis, T. S., Galyov, E. E., and Majerus, P. W. (1998) SopB, a protein required for virulence of *Salmonella dublin*, is an inositol phosphate phosphatase. *Proc. Natl. Acad. Sci. U.S.A.* **95,** 14057–14059
41. Wishart, M. J., and Dixon, J. E. (2002) PTEN and myotubularin phosphatases: from 3-phosphoinositide dephosphorylation to disease. *Trends Cell Biol.* **12,** 579–585
42. Grundner, C., Ng, H. L., and Alber, T. (2005) *Mycobacterium tuberculosis* protein tyrosine phosphatase PtpB structure reveals a diverged fold and a buried active site. *Structure* **13,** 1625–1634
43. Beresford, N., Patel, S., Armstrong, J., Szöor, B., Fordham-Skelton, A. P., and Tabernero, L. (2007) MptpB, a virulence factor from *Mycobacterium tuberculosis*, exhibits triple-specificity phosphatase activity. *Biochem. J.* **406,** 13–18
44. Tiaden, A., Spirig, T., Weber, S. S., Brüggemann, H., Bosshard, R., Buchrieser, C., and Hilbi, H. (2007) The *Legionella pneumophila* response regulator LqsR promotes host cell interactions as an element of the virulence regulatory network controlled by RpoS and LetA. *Cell Microbiol.* **9,** 2903–2920
45. Studier, F. W. (2005) Protein production by auto-induction in high density shaking cultures. *Protein Expr. Purif.* **41,** 207–234
46. Chen, J., de Felipe, K. S., Clarke, M., Lu, H., Anderson, O. R., Segal, G., and Shuman, H. A. (2004) *Legionella* effectors that promote nonlytic release from protozoa. *Science* **303,** 1358–1361
47. Kessler, A., Schell, U., Sahr, T., Tiaden, A., Harrison, C., Buchrieser, C., and Hilbi, H. (2013) The *Legionella pneumophila* orphan sensor kinase LqsT regulates competence and pathogen-host interactions as a component of the LAI-1 circuit. *Environ. Microbiol.* **15,** 646–662
48. Puhl, A. A., Gruninger, R. J., Greiner, R., Janzen, T. W., Mosimann, S. C., and Selinger, L. B. (2007) Kinetic and structural analysis of a bacterial protein tyrosine phosphatase-like *myo*-inositol polyphosphatase. *Protein Sci.* **16,** 1368–1378
49. Heidtman, M., Chen, E. J., Moy, M. Y., and Isberg, R. R. (2009) Large-scale identification of *Legionella pneumophila* Dot/Icm substrates that modulate host cell vesicle trafficking pathways. *Cell Microbiol.* **11,** 230–248
50. Burstein, D., Zusman, T., Degtyar, E., Viner, R., Segal, G., and Pupko, T. (2009) Genome-scale identification of *Legionella pneumophila* effectors using a machine learning approach. *PLoS Pathog.* **5,** e1000508
51. Zhu, W., Banga, S., Tan, Y., Zheng, C., Stephenson, R., Gately, J., and Luo, Z. Q. (2011) Comprehensive identification of protein substrates of the Dot/Icm type IV transporter of *Legionella pneumophila*. *PLoS One* **6,** e17638
52. Lifshitz, Z., Burstein, D., Peeri, M., Zusman, T., Schwartz, K., Shuman, H. A., Pupko, T., and Segal, G. (2013) Computational modeling and experimental validation of the *Legionella* and *Coxiella* virulence-related type-IVB secretion signal. *Proc. Natl. Acad. Sci. U.S.A.* **110,** E707–E715
53. Reeves, M. W., Pine, L., Hutner, S. H., George, J. R., and Harrell, W. K. (1981) Metal requirements of *Legionella pneumophila*. *J. Clin. Microbiol.* **13,** 688–695
54. Cianciotto, N. P. (2007) Iron acquisition by *Legionella pneumophila*. *Biometals* **20,** 323–331
55. Peracino, B., Balest, A., and Bozzaro, S. (2010) Phosphoinositides differentially regulate bacterial uptake and Nramp1-induced resistance to *Legionella* infection in *Dictyostelium*. *J. Cell Sci.* **123,** 4039–4051
56. Bozzaro, S., Buracco, S., and Peracino, B. (2013) Iron metabolism and resistance to infection by invasive bacteria in the social amoeba *Dictyostelium discoideum*. *Front. Cell Infect. Microbiol.* **3,** 50
57. Peracino, B., Buracco, S., and Bozzaro, S. (2013) The Nramp (Slc11) proteins regulate development, resistance to pathogenic bacteria and iron homeostasis in *Dictyostelium discoideum*. *J. Cell Sci.* **126,** 301–311
58. Segal, G., and Shuman, H. A. (1998) Intracellular multiplication and human macrophage killing by *Legionella pneumophila* are inhibited by conjugal components of IncQ plasmid RSF1010. *Mol. Microbiol.* **30,** 197–208
59. Sadosky, A. B., Wiater, L. A., and Shuman, H. A. (1993) Identification of *Legionella pneumophila* genes required for growth within and killing of human macrophages. *Infect. Immun.* **61,** 5361–5373
60. Wiater, L. A., Sadosky, A. B., and Shuman, H. A. (1994) Mutagenesis of *Legionella pneumophila* using Tn*903*dll*lacZ*: identification of a growth-phase-regulated pigmentation gene. *Mol. Microbiol.* **11,** 641–653
61. Mampel, J., Spirig, T., Weber, S. S., Haagensen, J. A. J., Molin, S., and Hilbi, H. (2006) Planktonic replication is essential for biofilm formation by *Legionella pneumophila* in a complex medium under static and dynamic flow conditions. *Appl. Environ. Microbiol.* **72,** 2885–2895
62. Kabsch, W. (2010) XDS. *Acta Crystallogr. D Biol. Crystallogr.* **66,** 125–132.
63. Adams, P. D., Afonine, P. V., Bunkóczi, G., Chen, V. B., Davis, I. W., Echols, N., Headd, J. J., Hung, L. W., Kapral, G. J., Grosse-Kunstleve, R. W., McCoy, A. J., Moriarty, N. W., Oeffner, R., Read, R. J., Richardson, D. C., Richardson, J. S., Terwilliger, T. C., and Zwart, P. H. (2010) PHENIX. A comprehensive Python-based system for macromolecular structure solution. *Acta Crystallogr. D Biol. Crystallogr.* **66,** 213–221
64. Emsley, P., and Cowtan, K. (2004) *Acta Crystallogr. D Biol. Crystallogr.* **60,** 2126–2132
65. Davis, I. W., Leaver-Fay, A., Chen, V. B., Block, J. N., Kapral, G. J., Wang, X., Murray, L. W., Arendall, W. B., 3rd, Snoeyink, J., Richardson, J. S., and Richardson, D. C. (2007) MolProbity. All-atom contacts and structure validation for proteins and nucleic acids. *Nucleic Acids Res.* **35,** W375–W383
66. Duarte, J. M., Srebniak, A., Schärer, M. A, and Capitani, G. (2012) Protein interface classification by evolutionary analysis. *BMC Bioinformatics* **13,** 334